Applied Catalysis B: Environmental 176–177 (2015) 11–19

Contents lists available at ScienceDirect

Applied Catalysis B: Environmental

journal homepage: www.elsevier.com/locate/apcatb

Novel MWNTs–Bi_2WO_6 composites with enhanced simulated solar photoactivity toward adsorbed and free tetracycline in water

Longfei Yue, Shanfeng Wang, Guoqiang Shan, Wei Wu, Liwen Qiang, Lingyan Zhu*

Key Laboratory of Pollution Processes and Environmental Criteria, Ministry of Education, Tianjin Key Laboratory of Environmental Remediation and Pollution Control, College of Environmental Science and Engineering, Nankai University, 300071 Tianjin, PR China

ARTICLE INFO

Article history:
Received 27 December 2014
Received in revised form 11 March 2015
Accepted 22 March 2015
Available online 24 March 2015

Keywords:
Photocatalysis
Multiwalled carbon nanotubes
Bi_2WO_6
Tetracycline
Adsorption

ABSTRACT

A novel three-dimensional (3D) mesoporous multiwalled carbon nanotubes-Bi_2WO_6 (MWNTs–Bi_2WO_6) microsphere photocatalyst with excellent photocatalytic performance was synthesized by a facile hydrothermal method and used to catalytically degrade tetracycline (TC) in water. Compared with pure Bi_2WO_6, the photocatalytic activity of the MWNTs–Bi_2WO_6 composites was enhanced significantly. The incorporated MWNTs facilitated the photogenerated electron transfer and enhanced the separation of photogenerated hole and electron pairs. In addition, the composite displayed stronger light absorption in the visible light region. Furthermore, the large surface as well as π–π electron coupling with the contaminants of MWNTs promoted the adsorption of TC on the photocatalyst surface. As a result, the incorporation of MWNTs with Bi_2WO_6 enhanced photocatalytic activity. The best photocatalytic performance was achieved with MWNTs proportion of 3%. Almost 100% of TC (20 mg/L) was removed by the solids of 3% MWNTs–Bi_2WO_6 (0.5 g/L) after irradiation with simulated solar light for 60 min and the degradation efficiency increased about 35% compared with the bare Bi_2WO_6. The degradation of the adsorbed TC on the catalyst was also investigated. The FT-IR and DTG analyses demonstrated that the adsorbed TC was slightly degraded in 1 h irradiation although the free TC in solution was completely degraded. As the irradiation extended for 3 h, the adsorbed TC was also degraded. The results indicated that the prepared MWNTs–Bi_2WO_6 composite has great potential for treatment of organic pollutants in water.

1. Introduction

Tetracycline (TC) is a widely used antibiotic and has become the second largest antibiotic used in the world [1,2]. The great amount of usage, especially the overuse and misuse in developing countries would lead to potential environmental problems. TC could be excreted through feces and urine as un-metabolized parent compound [3]. As a result, it is widely present in aquatic environment [4] and could be accumulated in biota, producing multi-resistant bacterial strains in the environment [3]. It is a great challenge to remove TC from waste and surface water.

Many different methods have been developed to remove TC, including physical, chemical and biological remediation strategies, among which, photocatalytic degradation attracts extensive attention due to its high efficiency and low cost. TiO_2 is the most widely used photocatalyst. However, TiO_2 can only make use 3–5% of solar light, which restricts its practical application. Recently, bismuth photocatalysts including Bi_2WO_6 have been developed for photocatalysis under visible light irradiation. Bi_2WO_6 is one of the simplest aurivillius metallic oxide with general formula $Bi_2A_{n-1}BnO_{3n+3}$ (A: Ca, Sr, Ba, Pb, Bi, Na, K and B: Ti, Nb, Ta, Mo, W, Fe) [5], which consists of $(Bi_2O_2)^{2+}$ and $(WO_4)^{2-}$ layers arranging alternatively and possesses excellent photocatalytic activity under visible light irradiation. To further improve the photocatalytic activity of Bi_2WO_6 some carbon materials such as graphene, fullerene (C_{60}), carbon nitride (C_3N_4) and carbon nanotubes (CNTs), which have delocalized conjugated π structures, could be incorporated with Bi_2WO_6 to accelerate the separation of the photogenerated charges, reduce the recombination of hole–electron pairs and then enhance the photocatalysis efficiency [6–8].

Multiwalled carbon nanotubes (MWNTs) have attracted considerable attentions due to their extraordinary electrical, chemical, and mechanical properties. The large surface area of MWNTs and capability of π–π electron coupling with organic contaminants promote the adsorption capacity to organic pollutants, boosting the removal efficiency [4]. In addition, the unique electronic properties of the MWNTs favor the charge transfer generated by

* Corresponding author at: The College of Environmental Science and Engineering, Nankai University, Weijin Road 94, Tianjin 300071, PR China. Tel.: +86 22 23500791; fax: +86 22 23508 807.
E-mail address: zhuly@nankai.edu.cn (L. Zhu).

http://dx.doi.org/10.1016/j.apcatb.2015.03.043
0926-3373/

semiconductors under light irradiation, prolonging the lifetime of electron–hole pairs. Thus, it is hypothesized that MWNTs is a good dopant to increase the photocatalytic capacity of catalysts [9–11]. However, to our knowledge, there is no report on the synthesis and photocatalytic activities of MWNTs–Bi_2WO_6 composites.

Though photocatalysis of organic pollutants has been widely studied, many studies focused on the pollutants in aqueous solution without considering the adsorbed fractions on the photocatalyst. In the previous studies [10–12], although high total removal efficiency of TC was reported, it remains unclear whether the adsorbed TC was degraded or not.

In the current study, MWNTs were coupled to Bi_2WO_6 using a simple hydrothermal method. The composites were applied to degrade TC in aqueous phase under the irradiation of simulated solar light. The interaction between MWNTs and Bi_2WO_6 as well as the mechanisms of enhanced photocatalytic activity were systematically investigated. Additionally, we tried to investigate the degradation of adsorbed TC using different analytical methods.

2. Experimental

2.1. Materials and reagents

MWNTs (10–30 nm diameter, 5–15 nm length, purity > 98%) were purchased from Shenzhen Nanotech Port, China. NaOH (AR) and HNO_3 (AR, 65%) were purchased from Jiangtian Chemical Technology Co., Ltd., Tianjin, China. TC (GR), $Bi(NO_3)_3{\cdot}5H_2O$ (AR), $Na_2WO_4{\cdot}4H_2O$ (AR), ammonium oxalate (AR), KI (AR) and $AgNO_3$ (AR) were purchased from GuangFu Technology Development Co., Ltd. Isopropanol (AR) and methanol (AR) were purchased from Concord Technology Co., Ltd. The TiO_2 particles (Rutile and Anatase) were purchased from Aladdin industry corporation and TiO_2 particles (P25, Degussa) were purchased from Degussa Corporation, Germany.

2.2. Purification of MWNTs and photocatalysts preparation

Amorphous carbon, fullerene and carbon nanoparticles are the common impurities in the raw MWNT materials. A purification method reported by Song et al. [11] was used to remove the impurities. Five g of MWNT and 300 mL of 65% HNO_3 were added in a 500 mL round-bottom flask. After ultrasonication for 5 min, the solution was refluxed for 2 h, then cooled down to room temperature. The mixture was filtered and washed with deionized water until the pH of the solution was nearly 7. The dark precipitates were collected, which were then dried in an oven at 90 °C for 8 h.

A typical hydrothermal method, which was reported by Wang et al. [13] was used to prepare the photocatalysts. 20 mL of 0.1 mol/L Bi $(NO_3)_3$ solution was used as the source of bismuth. A desired amount of MWNTs was added, resulting in the mass ratio of MWNT: Bi_2WO_6 as 0.3%, 1.5%, 3%, 5% and 10%. 20 mL of Na_2WO_4 solution (0.05 mol/L) was added dropwisely under stirring. The mixture was stirred for 10 min and ultrasonicated for 30 min. The pH of the suspension was adjusted by NaOH or HNO_3 solutions to about 1 and transferred to a 50 mL of Teflon-lined autoclave and heated in an oven at 140 °C for 20 h. The solids were collected and washed by deionized water and absolute ethanol consecutively and then dried under 80 °C for one night in oven. The color of the solids varied from gray to black as the ratio of MWNTs: Bi_2WO_6 increased. The resultant catalysts were defined as 0.3%, 1.5%, 3%, 5% and 10% MWNTs–Bi_2WO_6.

2.3. Photocatalysts characterization

The X-ray diffraction (XRD) was carried on D/MAX 2500 V diffractometer (Rigaku, Japan) with monochromatized Cu Kα radiation under 40 kV and 100 mA and the scanning range was from 10 to 80°. The morphologies and microstructures of the products were characterized by a field emission scanning electron microscopy (FE-SEM, LEO, 1530vp, Germany), and a high-resolution transmission electron microscopy (HR-TEM, JEM-2010FEF, Japan). The X-ray photoelectron spectroscopy (XPS, Kratos Axis Ultra DLD) using monochromatized Al Kα X-ray as the excitation source was applied to study the composition and chemical state of the elements. The FT-IR spectra were carried out on MAGNA-560 Nicolet. UV–vis diffuse reflectance spectra (DRS) of the samples were tested on a Hitachi U-3010 spectrometer. The spectra were recorded in the range of 200–800 nm. The surface areas were measured by the Brunauer–Emmett–Teller (BET) method, and the average pore diameter was obtained from the sorption/desorption isotherms of N_2 using the Barrett–Joyner–Halenda (BJH) equation by surface area and porosimetry analyzer (TriStar 3000, Micromeritics, USA). Thermogravimetry (TG) and derivative thermogravimetry (DTG) were measured by (NETZSCH TG209 Germany). The samples were subjected to a linear temperature change of 10.0 (K/min) under the N_2 air.

Photoelectrochemical measurement was carried out using an electrochemical analyzer (Chenhua Instruments Co., Shanghai) with conventional three-electrodes and the ITO/photocatalyst electrodes as the working electrode, a Pt wire as the counter electrode and saturated calomel electrode Ag/AgCl (saturated KCl) as a reference electrode. The 0.1 M Na_2SO_4 was used as electrolyte which was filled in a single-compartment quart cell. The photoresponses of the photocatalysts were measured at 0.0 V as visible light ($\lambda > 400$ nm) was switched on and off [14].

2.4. Adsorption and degradation experiments

Adsorption and degradation experiments were conducted in a XPA-7 photochemical reactor (Xujiang Electromechanical plant, Nanjing, China). Simulated sunlight irradiation was obtained from a 800 W Xenon lamp (Institute for Electric Light Sources, Beijing) without the cutoff filter. The reaction system was cooled by circulating water to maintain at room temperature. 20 mL of TC solution (20 mg/L) was put in 50 mL quartz test tubes. A certain amount of photocatalysts were added in the solution with constant magnetic stirring. After 30 min magnetic stirring to establish the adsorption–desorption equilibrium of TC on the catalysts, the Xenon lamp was switched on to initiate irradiation. An aliquot (1 mL) was sampled at certain time intervals, which was then centrifuged at 8000 rpm to remove the particles before analysis by a high performance liquid chromatography (HPLC).

2.5. Instrumental analysis

TC was analyzed using a HPLC (Agilent 1260 infinity, Agilent Corporation, USA) with a VWD detector (Wavelength was at 355 nm) and the column was a Waters XTerra MS C18 (particle size 5 μm, 2.1 × 150 mm). The analytical conditions were as follows: the mobile-phase was 65% methanol and 35% water (with 0.225% glacial acetic acid) with a flow rate of 0.2 mL/min. The oven temperature was at room temperature.

3. Results and discussion

3.1. Compositions of the photocatalysts and effects of loading amount of MWNTs on the photodegradaion efficiency

Fig. 1a shows the XRD patterns of the catalysts prepared with different contents of MWNTs. All the diffraction peaks could be well indexed to orthorhombic Bi_2WO_6 crystal phase (JCPDS Card No. 39-0256) with $a = 5.457$ Å, $b = 16.435$ Å, $c = 5.438$ Å [15], suggesting that

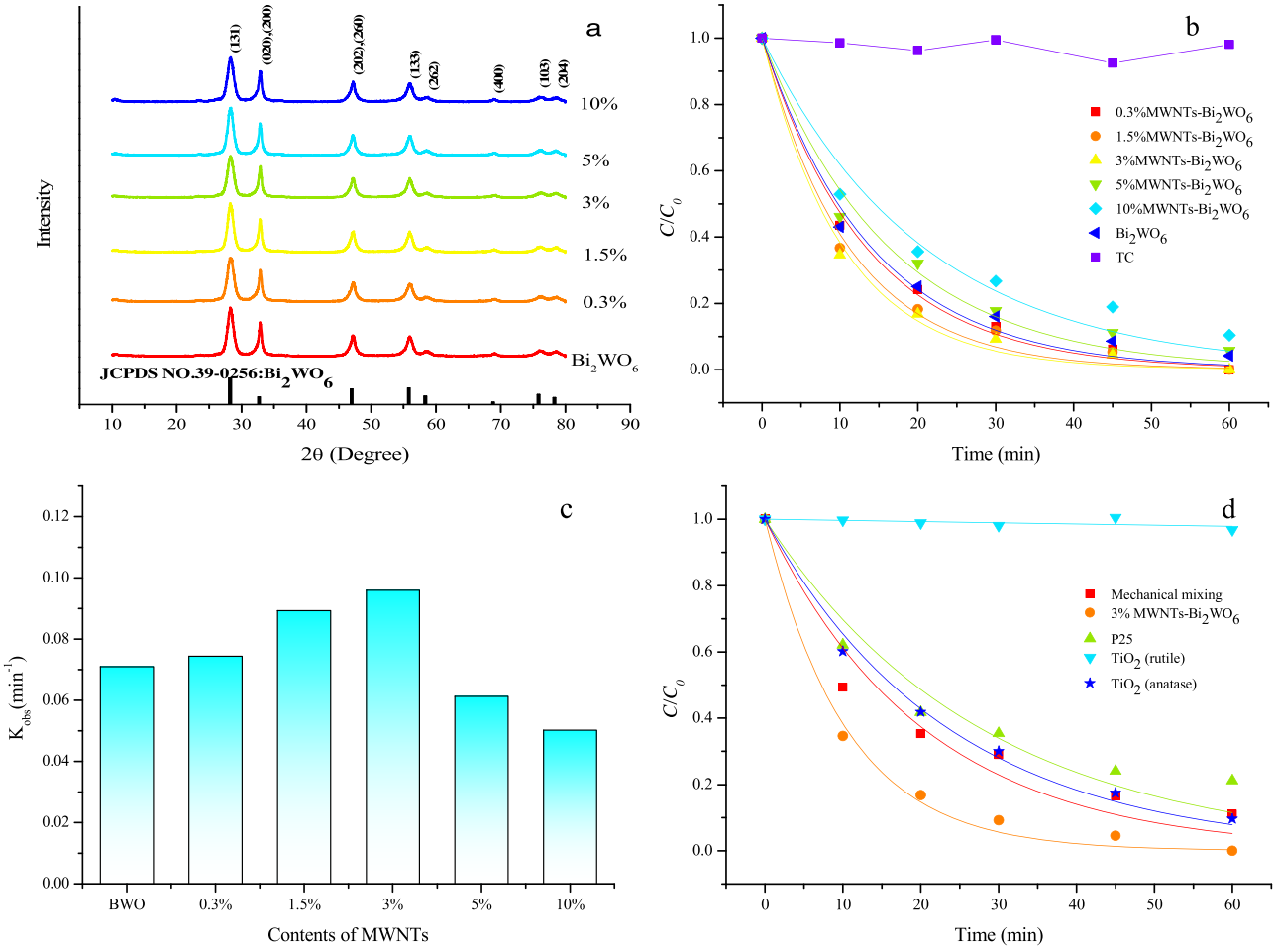

Fig. 1. (a) The XRD patterns of the prepared materials; (b and c) The photocatalytic efficiency and rate constant (K_{obs}) with the prepared photocatalysts containing different load of MWNTs. (Photocatalysts with 0%, 0.3%, 1.5%, 3%, 5%, 10% MWNTs, 0.5 g/L, irradiation time 60 min; TC concentration 20 mg/L); (d) The photocatalytic efficiency of different catalysts (including mechanic mixture of Bi_2WO_6 and 3% MWNTs, 3% MWNTs–Bi_2WO_6, P25, anatase and rutile TiO_2, 0.5 g/L, irradiation time 60 min, TC concentration 20 mg/L).

the catalysts had similar crystallite size and crystallinity. The doping with MWNTs did not significantly change the structure of the Bi_2WO_6. It was reported that MWNTs had a weak but characteristic diffraction peak at 26.0°. However, this peak was not apparent for the as-prepared composites, which could be attributed to the small amount of MWNTs in the composites [16]. On the other hand, the (131) diffraction peak of Bi_2WO_6 could also overlap with the characteristic peak at 26.0°.

Fig. 1b illustrates the reaction kinetics of TC and the following pseudo-first-order reaction kinetic model (Eq. (1)) could be well used to describe the reaction kinetics with regression coefficient $R^2 > 0.9667$ [17].

$$\frac{C_t}{C_0} = e^{-k_{obs}t} \quad (1)$$

where C_0 and C_t are TC concentrations in aqueous phase (mg/L) at beginning and reaction time t. K_{obs} is the pseudo-first-order rate constant (min^{-1}) and t is reaction time (min).

In the control test without any catalysts, only around 5% of TC was degraded under simulated solar irradiation for 60 min, implying that TC is very stable under solar light irradiation. The photocatalytic activity increased gradually with increasing the amount of MWNTs in the composite and the highest photocatalytic rate constant K_{obs} (0.0959 min^{-1}) was achieved with 3% MWNTs–Bi_2WO_6 (Fig. 1c), which increased by 35% compared with that of pure Bi_2WO_6 (0.07105 min^{-1}). As the proportion of MWNTs in the composite further increased, the degradation efficiency gradually decreased. This could be due to that more MWNTs might block the pores of the composites and reduce the active sites of Bi_2WO_6. As a result, the photodegradation efficiency of the photocatalyst decreased [18]. Thus the 3% MWNTs–Bi_2WO_6 was selected for the following study.

To illustrate the impact of hybridization of MWNTs with Bi_2WO_6 on the photodegradation of TC, the photodegradation efficiency of the 3% MWNTs–Bi_2WO_6 was compared with other materials, including the physical mixture of Bi_2WO_6 and 3% MWNTs, anatase, rutile and P25 TiO_2. As shown in Fig. 1d, rutile TiO_2 displayed negligible catalytic effect on the photodegradation of TC, and those of anatase, P25 TiO_2 and the mixture of Bi_2WO_6 and 3% MWNTs were much lower than the 3% MWNTs–Bi_2WO_6 composite, suggesting that the chemical interaction between MWNTs and Bi_2WO_6 in the composites is sufficient for enhancing the photocatalytic activity [6].

3.2. Mechanisms for the enhanced photoactivity of the 3% MWNTs–Bi_2WO_6

A variety of characterization techniques were used to explore the mechanisms for the enhanced photocatalysis efficiency of the composites. Fig. 2 illustrates the field emission scanning electron microscopy (FESEM) of the 3% MWNTs–Bi_2WO_6. In the FESEM image at low magnification in Fig. 2a, the 3% MWNTs–Bi_2WO_6

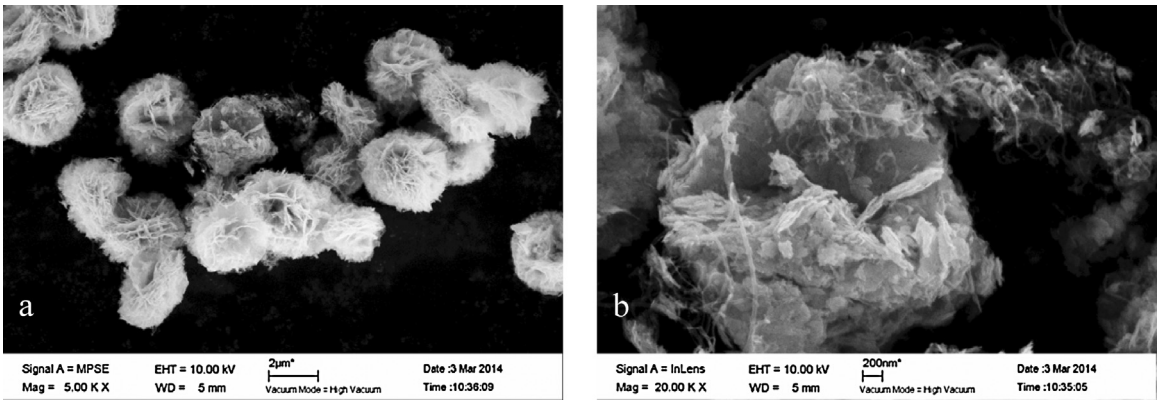

Fig. 2. The FESEM images of 3% MWNTs–Bi_2WO_6. (a) low magnification; (b) high magnification.

composite exhibited uniform and microsphere-like architectures ranging from 1 to 3 μm in diameter. The three dimensional (3D) microspheres were assembled by nanosheets of Bi_2WO_6 with thickness of 10–30 nm. In Fig. 2b with high magnification, the MWNTs were visible and they were interlaced between the Bi_2WO_6 nanosheets. The good attachment of MWNTs with the microspheres would favor the separation of photogenerated hole–electron pairs due to the excellent mobility of charge carriers on the MWNTs surface [19]. On the other hand, MWNTs could provide more active sites for TC adsorption, which improved the contact of TC with Bi_2WO_6 and then degradation efficiency [11].

The microstructures of the as-prepared samples were further analyzed using transmission electron microscopy (TEM) and high resolution transmission electron microscopy (HRTEM), as shown in Fig. 3a. Agreeing with FESEM, the Bi_2WO_6 nanosheets integrated with each other to form sphere-like structure, and MWNTs were interlaced among them. Fig. 3b shows the HRTEM image taken for the junction of the two components, Bi_2WO_6 and MWNTs. The lattices of the two components intersected each other, confirming the successful incorporation of MWNTs with Bi_2WO_6. In Fig. 3c, the interplanar spacing was determined to be 0.274 nm, corresponding to the (0 2 0) and (2 0 0) planes of the Bi_2WO_6. This result was in well accordance to the XRD results in which the intensity of (0 2 0) or (2 0 0) was stronger than that of the standard pattern. In addition, the corresponding fast Fourier transform (FFT) pattern inserted in Fig. 3c shows a single-crystalline pattern with sharp diffraction spots [20], indicating the high-crystallinity and good orthorhombic phase of the synthesized composites.

To investigate the surface compositions and chemical states of the synthesized composites, XPS was carried out and the results are displayed in Fig. 4. The binding energies were calibrated using C 1s peak of aliphatic carbon at 284.6 eV. The full scan results in Fig. 4a indicate that Bi, O, W and C elements were present in pure Bi_2WO_6 and the 3% MWNTs–Bi_2WO_6 composite. The C element detected in Bi_2WO_6 was due to the adventitious hydrocarbon of the XPS instrument [21]. The spectrum of the MWNTs indicates that it contained only C and O elements. Fig. 4b–f display the high-resolution spectra of the Bi 4f, W 4f, O 1s and C 1s, respectively. The spin–orbit of the Bi 4f of Bi_2WO_6 could be well deconvoluted as two peaks at 159.004 and 164.320 eV, which are corresponding to the Bi $4f_{7/2}$ and Bi $4f_{5/2}$ orbits of Bi^{3+}. The peaks in Fig. 4c at 35.139 and 37.223 eV could be assigned to W $4f_{7/2}$ and W $4f_{5/2}$, indicating the existence of W^{6+} oxidation state. The deconvoluted peaks at 532.999 and 529.758 eV of O 1s in Fig. 6d were consistent with the different chemical environments of oxygen element in Bi—O [22] and W—O [21]. The peak at 531.000 eV corresponded to the hydroxyl groups on the surface of Bi_2WO_6 [23]. In the case of 3% MWNTs–Bi_2WO_6, the binding energy of both Bi 4f and W 4f shifted about 0.1–0.2 eV toward lower binding energies. Similar result also happened to O 1s. This implied the successful incorporation of MWNTs with Bi_2WO_6 [24], which changed the chemical environment of these elements. Fig. 4e displays the deconvolution of the C 1s peak of pure MWNTs. The main peak at 284.6 eV was assigned to sp^2-hybridized carbon from the MWNTs, which refers to the C—C bond of the sp^2-hybridized carbon in the graphene sheet. The peak at 285.037 eV was attributed to the defects-containing sp^2-hybridized carbon on the nanotube structure [25]. The peak at 282.532 eV was assigned to the C=C bond. In addition, the peaks located at 285.594, 287.209 and 288.887 eV corresponded to C—O, C=O, O—C=O respectively [25,26]. The peak at 291.008 eV was featured as π–π^* transition [27]. In Fig. 4f, unlike the spectra of pure MWNTs, the C 1s spectra of the 3% MWNTs–Bi_2WO_6 could only be deconvoluted as three peaks, 284.6, 286.266 and 288.538 eV, which were ascribed to C—O and C=O or COO bonds, respectively. Other

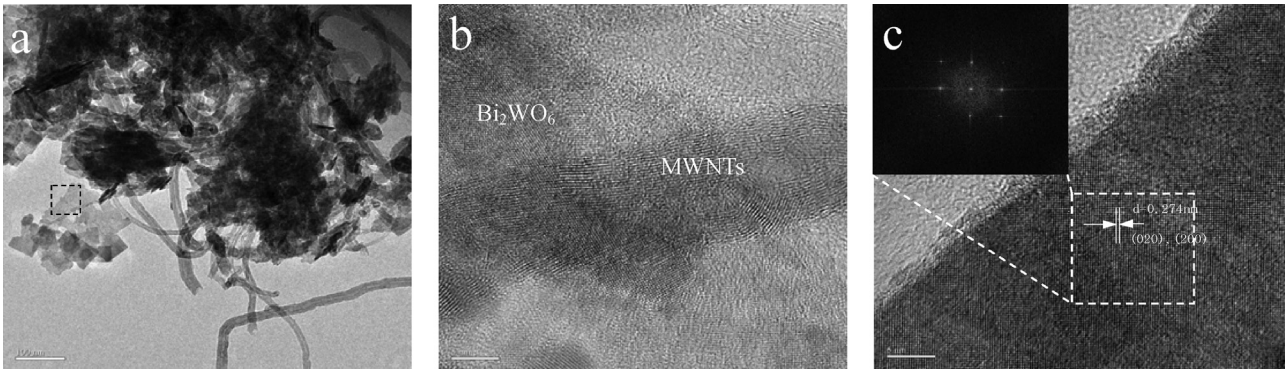

Fig. 3. (a and b) The TEM images of 3% MWNTs–Bi_2WO_6; (c) HRTEM images of 3% MWNTs–Bi_2WO_6.

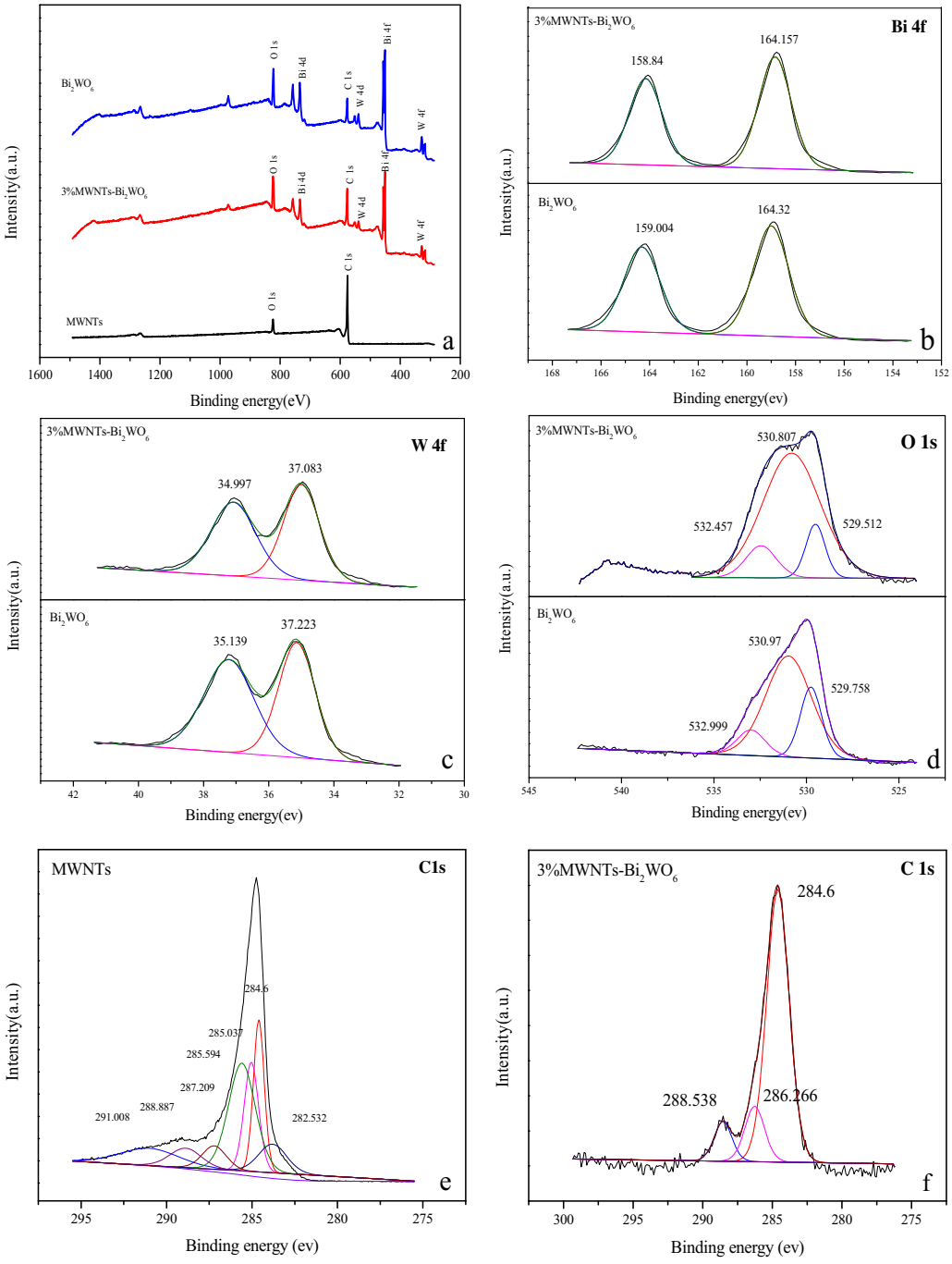

Fig. 4. The XPS spectra of the MWNTs, Bi_2WO_6 and 3% MWNTs–Bi_2WO_6 composite. (a) Full scan; (b) Bi 4f; (c) W 4f; (d) O 1s; (e) C 1s of MWNTs; and (f) C 1s of 3% MWNTs–Bi_2WO_6.

peaks of C 1s were not identified, which could be due to the small amount of MWNTs in the composites, leading to trace amount of C on the surface and very weak signals.

Table 1 lists the binding energies and relative area ratios of different peaks. As compared with pure Bi_2WO_6, the peak area ratio of W $4f_{7/2}$ and W $4f_{5/2}$ in the composite increased about 4%, while the ratio of Bi $4f_{7/2}$ and Bi $4f_{5/2}$ peaks did not change much. Similarly, the peak ratio of W—O peaks decreased 10.92%, while that of the Bi—O peak did not change. Besides, the binding energy of C—O as well as the intensities of the C—C and C—O bonds changed significantly. These results suggested that there was chemical rather than physical interaction between MWNTs and Bi_2WO_6, mainly among the C atoms of MWNTs and the O and W elements in Bi_2WO_6. It is well known that the conduct band of Bi_2WO_6 is made up of the W 5d orbit. When the photocatalyst is irradiated, the hole–electron pairs on valence band will be inspired and the electrons will transfer to the conduct band. The successful incorporation between the C and W elements would favor the transfer of electrons from the conduct band of Bi_2WO_6 to MWNTs

Fig. 5a shows the PL spectra of pure Bi_2WO_6 and 3% MWNTs–Bi_2WO_6 composite at an excitation wavelength of 325 nm. Their emission bands centered at about 480–500 nm [28]. The emission intensity of the 3% MWNTs–Bi_2WO_6 was only half of that of pure Bi_2WO_6. This suggests that incorporation of MWNTs reduced the charge recombination rate due to efficient transfer of

Table 1
Peak position, area and percentage of each XPS peak among the total XPS peaks of one specific element.

	Bi_2WO_6						MWNTs		
Peak	W $4f_{7/2}$	W $4f_{5/2}$	Bi $4f_{7/2}$	Bi $4f_{5/2}$	W—O	Bi—O	C—C	C—O	COO
Position(eV)	35.139	37.223	159.004	164.320	529.758	532.999	284.600	285.594	288.887
Area (%)	22692	24962	175128	137351	23080.9	11045.7	27525.5	48595.5	10368.5
Percentage	47.68%	52.32%	56.03%	43.97%	22.19%	10.61%	19.54%	34.49%	7.36%
	3% MWNTs–Bi_2WO_6								
Peak	W $4f_{7/2}$	W $4f_{5/2}$	Bi $4f_{7/2}$	Bi $4f_{5/2}$	W—O	Bi—O	C—C	C—O	COO
Position(eV)	34.997	37.083	158.840	164.157	529.512	532.457	284.600	286.266	288.538
Area (%)	18621.8	17672.0	130480	101668	11837.2	11164.0	39941.4	4594.3	7134.0
Percentage	51.37%	48.63%	56.19%	43.81%	11.27%	10.63%	77.30%	8.89%	13.81%

photoexcited electrons from the conduct band of Bi_2WO_6 to MWNTs which was described in the XPS analysis.

Fig. 5b illustrates the transient photocurrent responses of Bi_2WO_6 and 3% MWNTs–Bi_2WO_6 electrodes. The photocurrent response of the 3% MWNTs–Bi_2WO_6 appeared to be two times higher than that of pure Bi_2WO_6 under light irradiation, supporting that there were less recombination and more efficient separation of photogenerated electron–hole pairs for 3% MWNTs–Bi_2WO_6 composite. The shape of the photocurrent of Bi_2WO_6 was different from that of the 3% MWNTs–Bi_2WO_6: a small peak was observed as the light switched on for Bi_2WO_6 but this was not the case for 3% MWNTs–Bi_2WO_6. This peak could be attributed to the separation of photoinduced electron–hole pairs at the surface of the photocatalyst [29]. After the peak current, a gradual decay was observed until it reached a constant photocurrent, which was mainly due to the recombination of the photogenerated charges. The decay could be also attributed to that the electrons were oxidized by some active species in the electrolyte. For the 3% MWNTs–Bi_2WO_6 composite, there was no such peak and the transient photocurrent was quite constant [30]. MWNTs could act as the electron trap which would lead to dull response of photocurrent as the light switched on or off [29]. All of these suggest that MWNTs could effectively separate the photoinduced electron–hole pairs.

The porous structures and BET surface areas of the 3% MWNTs–Bi_2WO_6 composite and pure Bi_2WO_6 are illustrated in Fig. S1. Both isotherms were characteristic of type IV with typical H3 hysteresis loops observed in the range of 0.50–1.00 P/P_0 [31,32], indicating the mesoporous structures of the photocatalysts. The pores were mainly in the range of 0–30 nm. The main peaks at 7 nm for pure Bi_2WO_6 and 10 nm for the composites could be formed due to the stack of the Bi_2WO_6 nanosheets. The smaller peak at 3 nm in the composites might be attributed to the pores inside the MWNTs. The BET surface areas (S_{BET}) of pure Bi_2WO_6 and 3% MWNTs–Bi_2WO_6 were 19.63 and 43.32 m^2/g, respectively. The BJH absorption cumulative volume of the pores increased from 0.13 to 0.19 cm^3/g after incorporation with MWNTs.

The larger BET surface area of 3% MWNTs–Bi_2WO_6 would supply more adsorption sites, which would increase the adsorption of TC on the surface of the composites. The results displayed in Fig. S2 indicated that 31.3% of TC was adsorbed on the surface of 3% MWNTs–Bi_2WO_6 while only 21.8% of TC was adsorbed by pure Bi_2WO_6. The enhanced adsorption due to the large surface area would contribute to the higher degradation efficiency of 3% MWNTs–Bi_2WO_6.

The diffuse reflectance absorption spectra (DRS) of Bi_2WO_6 and MWNTs–Bi_2WO_6 composites with different contents of MWNTs were displayed in Fig. S3a. The UV–vis spectra changed significantly as MWNTs were incorporated with Bi_2WO_6. The incorporation of MWNTs significantly enhanced the absorption in the visible light region while depressed the absorption in the UV region. The increased absorption in the visible light could be due to the electronic transition of π–π^* of MWNTs, which influenced the formation process of electron–hole pairs and their separation under visible-light irradiation [33–35]. On the other hand, the MWNTs could shield the UV light, leading to lower absorbance in the UV region. The stronger absorption of 3% MWTNs-Bi_2WO_6 in the visible light regions would enhance the production of photoinduced

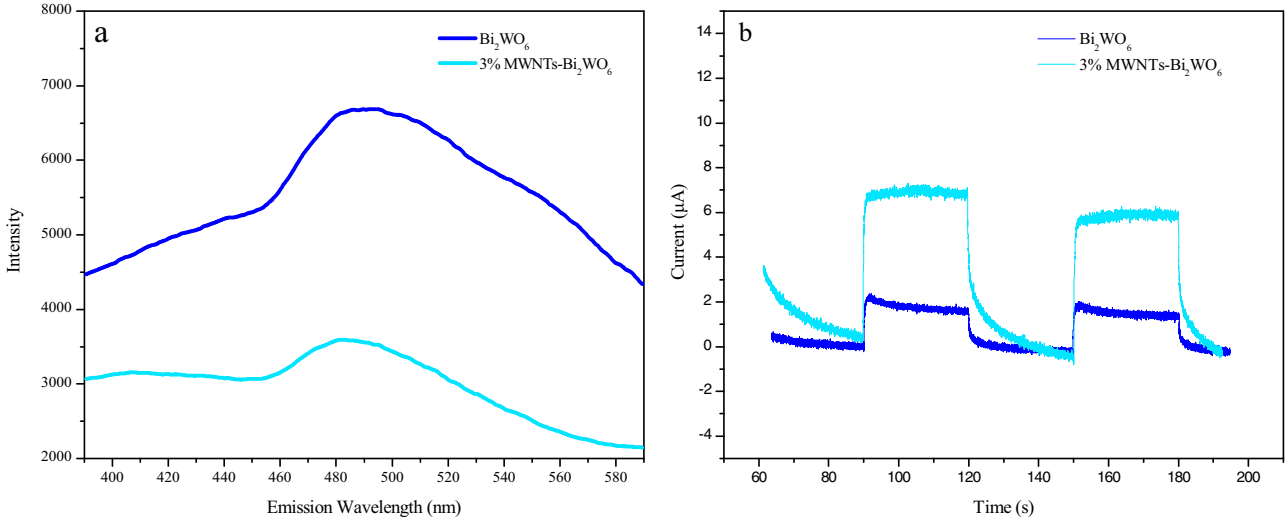

Fig. 5. (a) PL spectra of pure Bi_2WO_6 and 3% MWNTs–Bi_2WO_6 composite; (b) transient photocurrent responses of pure Bi_2WO_6 and 3% MWNTs–Bi_2WO_6.

hole–electrons and improve the photodegradation efficiency consequently.

For the crystalline semiconductor, pure Bi_2WO_6, the optical band gap could be calculated by the Tauc plot of the modified Kubelka–Munk (KM) function. The band gap of pure Bi_2WO_6 was determined as 2.53 eV and the edge potential of valence band (E_{VB}) and conduct band (E_{CB}) were calculated to be around 3.16 and 0.63 eV. The detailed calculation process is presented in Supporting information.

3.3. Degradation of TC adsorbed on the composites under simulated solar light irradiation

As illustrated in Fig. 6a, the FT-IR spectra of the 3% MWNTs–Bi_2WO_6 composite and pure Bi_2WO_6 were similar to each other, which was reasonable since Bi_2WO_6 was predominant in the composite. After adsorption with TC, the spectrum of the composite changed. Several new peaks appeared in the region of 1000 ~ 1400 cm^{-1} due to the adsorption of TC on the surface. By comparison with the FT-IR spectrum of TC (shown in Fig. S5), it is clear that the new peaks corresponded to the stretching vibration of the bonds, which were labeled by dashed lines in Fig. S5, in TC molecules. The spectra of the composite after adsorption of TC and after degradation for 1 h were similar to each other, implying that adsorbed substance on the surface was still TC after irradiation for 1 h. However, after irradiation for 3 and 5 h, the spectra changed distinctly with the disappearance of the peaks at 1200 ~ 1250 cm^{-1} and 1300 ~ 1350 cm^{-1}, which were assigned to C—N amine stretching vibration and —CH_3 deformation vibration [36], respectively. The disappearance of these two peaks implies that the adsorbed TC was degraded and transformed to some intermediate products through losing the —CH_3, —NH_2 or —$N(CH_3)_2$.

Fig. 6b illustrates the TG and DTG curves of Bi_2WO_6 and the composite at different reaction stages. The TC curves of the composite were much different from the pure Bi_2WO_6 and varied with the reaction time. To better understand the TG results of the materials, DTG curves were applied, which were the results of first derivative of TG, and widely applied to distinguish different pyrolysis substances through the changes of different peaks [37]. For the 3% MWNTs–Bi_2WO_6 composite and pure Bi_2WO_6, the peaks at around 300 ~ 400 °C (peak 1) could be due to loss of the adsorbed water. The peak at about 600–700 °C for 3% MWNTs–Bi_2WO_6 (peak 2), which was not observed for Bi_2WO_6, was attributed to the loss of MWNTs. The curve of the composite with adsorption of TC was different from the composite alone. The positions of peaks 1 and 2 moved to lower temperature, apparently due to the decomposition of the adsorbed TC, which agrees with the results stated above. The DTG curve of the composite after irradiation for 1 h was similar to that with adsorption of TC, supporting that TC was still on the surface of the composite after irradiation for 1 h even though TC in the solution was almost completely degraded. However, distinct changes were observed in the DTG curves of the composite after irradiation for 3 and 5 h. Two new peaks, peaks 3 and 4 emerged, implying the adsorbed substances on the composite were not TC anymore. It is well accepted that the photocatalytic degradation happened on or near the surface of the catalysts. Once the adsorbed TC was degraded on the surface of 3% MWNTs–Bi_2WO_6, some TC molecules in the solution would replace the sorption sites on the surface. As a result, the concentration of TC in the solution decreased gradually, while the surface concentration did not change during the first hour irradiation. As the irradiation continued, TC in the solution was degraded and some intermediates were produced. With the degradation going on, some sorption sites were released and

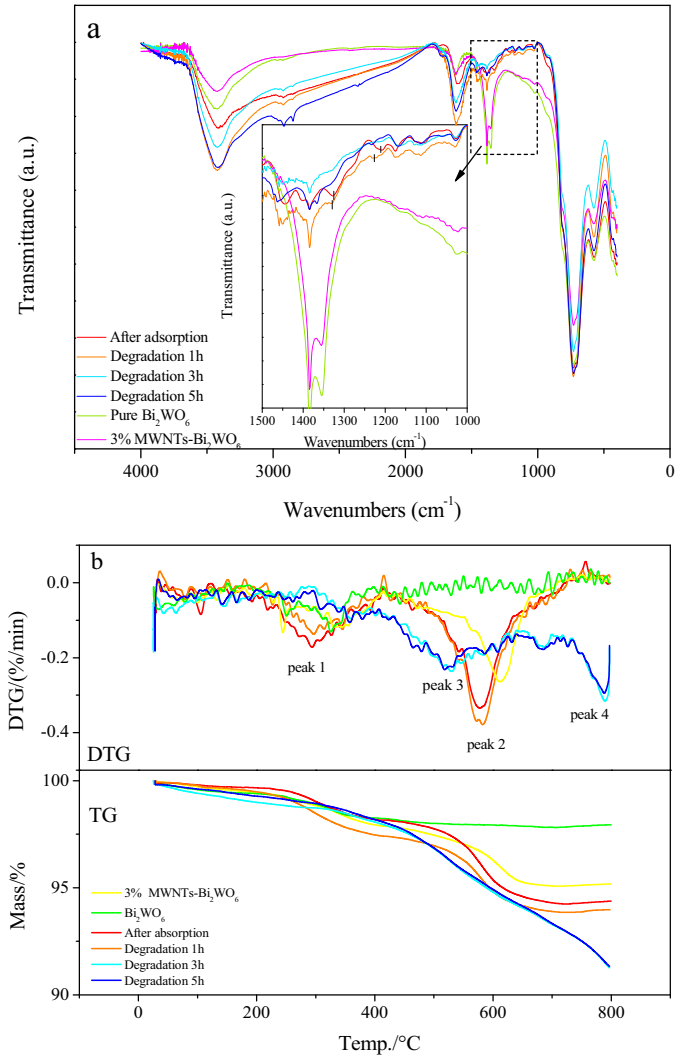

Fig. 6. (a) FT-IR spectra of the prepared 3% MWNTs–Bi_2WO_6 after adsorption but without irradiation, irradiation for 1 h, 3 h and 5 h, 3% MWNTs–Bi_2WO_6 composites, pure Bi_2WO_6 (b) TG and DTG curves of the prepared Bi_2WO_6 and 3% MWNTs–Bi_2WO_6 after adsorption of TC for 30 min and irradiation for 0, 1, 3 and 5 h.

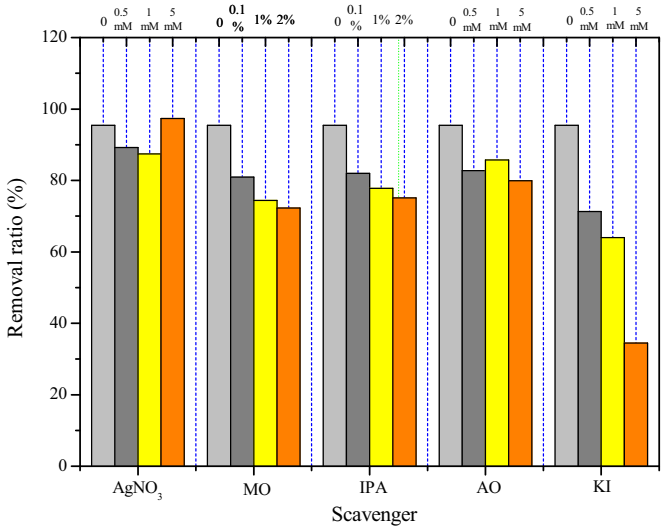

Fig. 7. Effects of different scavengers on degradation of TC (3% MWNTs–Bi_2WO_6 0.5 g/L, TC 20 mg/L; irradiation time 45 min).

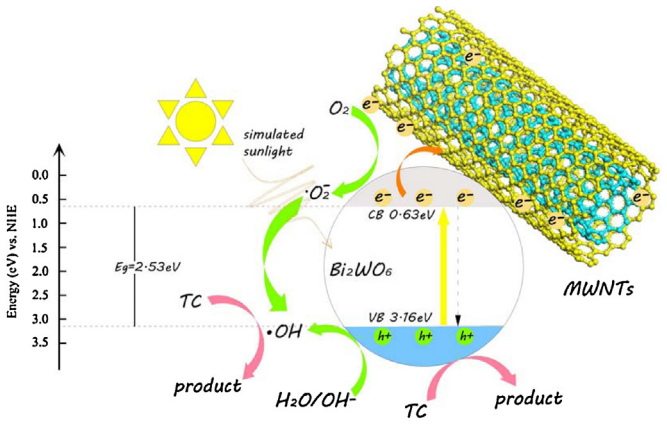

Fig. 8. Schematic diagram of energy bands of MWNTs–Bi_2WO_6 and the transfer of photogenerated charges in the MWNTs–Bi_2WO_6 under simulated sunlight.

occupied by the intermediates. Thus, new peaks were observed on the surface.

3.4. Photocatalytic reaction mechanisms

To examine the photocatalytic reaction mechanisms responsible for the degradation of TC under simulated solar light, different scavengers were used to investigate the active species. $AgNO_3$ was added to capture e^-, methanol (MO) and isopropanol (IPA) were adopted to capture •OH, ammonium oxalate (AO) was introduced to capture h_{vb}^+ and potassium iodide (KI) was used to evaluate the contribution of both photogenerated holes and hydroxyl radicals [38]. Fig. 7 illustrates the removal rate of TC with various scavengers after 45 min irradiation. The degradation was not greatly affected by $AgNO_3$. In contrast, methanol depressed the degradation of TC and the depression effect increased with the concentration of methanol. IPA displayed similar results as methanol, implying that •OH might play a significant role on the photodegradation. After addition of AO, the TC removal rate decreased with increasing AO concentration. These results indicate the contribution of h_{vb}^+ can not be negligible. The pivotal role of degradation of TC might be attributed to the combined effects of •OH and h_{vb}^+. This conclusion was testified by the fact that addition of KI at different concentrations resulted in significant inhibition. The I^- could capture h_{vb}^+ and •OH simultaneously.

Fig. 8 illustrates the suggested mechanisms for the enhanced photocatalytic degradation of the MWNTs–Bi_2WO_6 composites. As the simulated solar light irradiated on the MWNTs–Bi_2WO_6 composites, Bi_2WO_6 was excited and the photoinduced electrons would transfer from the valence band (VB) to conduction band (CB), leaving h_{vb}^+ in VB. The photogenerated electrons transfer freely from Bi_2WO_6 to MWNTs [39], resulting in low recombination rate. The h_{vb}^+ would oxide water molecules to form hydroxyl radicals (•OH) as shown in Eq. (2). In addition, oxygen would be reduced to generate superoxide radical ($\cdot O_2^-$), which then would form •OH through a series of reactions. Both h_{vb}^+ and •OH were the reactive oxygen species (ROSs) responsible for the photocatalysis. Consequently, the prepared MWNT-Bi_2WO_6 composites exhibited higher photoactivity than the pure Bi_2WO_6.

$$h^+ + H_2O \rightarrow \cdot OH + H^+ \quad (2)$$

3.5. The impact of solution pH on TC degradation

It has been reported that the initial pH of the aqueous solution might influence the generation of ROSs and have a great effect on photocatalytic reaction [17,40,41]. As shown in Fig. 9a, the photodegradation efficiency increased gradually as the pH increased from 1 to 11. As discussed above, •OH was one of the main active species responsible for TC photodegradation. The alkaline environment favors the production of •OH, resulting higher degradation efficiency at alkaline conditions. On the other hand, TC is amphoteric with pK_a values of 3.3, 7.7, 9.7 and 12 [42], as illustrated in Fig. S4. At pH < 4, it is mostly protonated as TC^+; at pH 4 ~ 7.5, it is mainly in neutral form TC^0 and the mono anionic form TC^- would dominate at pH 7.5 ~ 10.0. The electronic density of TC increased as pH increased, also favoring the attack of radical species on the molecules [43].

In addition, TC would become unstable as the pH increased from 1 to 11. As shown in Fig. 9b, the photolysis efficiency of TC increased as the initial pH increased, indicating that TC was prone to photolysis at alkaline conditions. This could be explained by the light absorption of TC at different pH conditions. Fig. 10 shows the UV–vis spectra of TC at different pHs. In pH 1–7, the peak positions of the main absorption were the same, yet the absorbance became stronger gradually, indicating the extinction efficiency of TC became lower. This suggests TC became less stable under light irradiation as the pH increased in the range of 1–7. As pH further increased, red shift of the absorption peak as well as increased

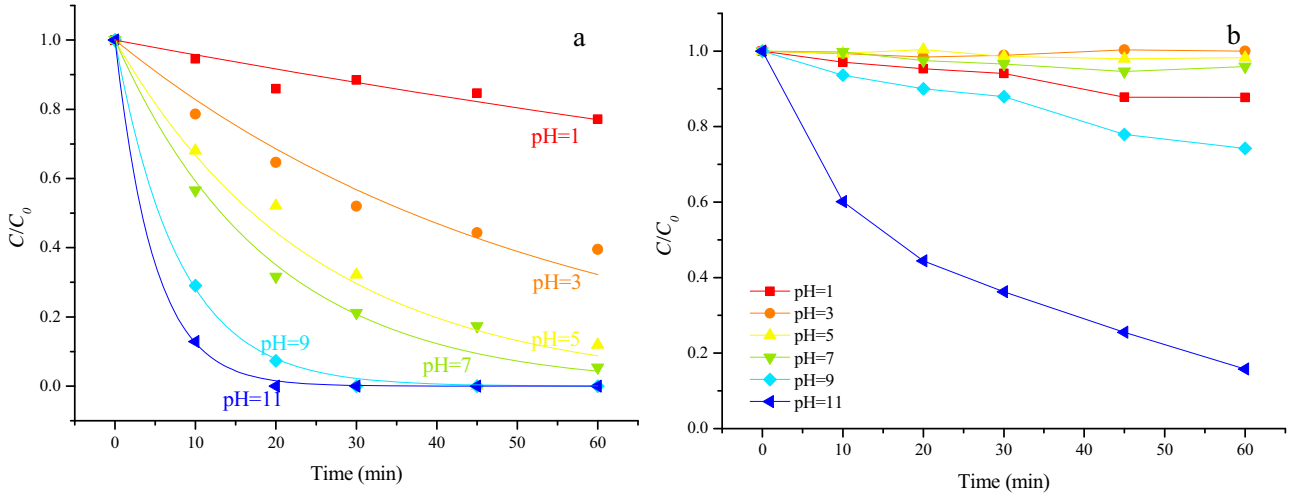

Fig. 9. (a) Influence of initial pH on the photocatalytic degradation of TC. (3% MWNTs–Bi_2WO_6 0.5 g/L, irradiation time 60 min); (b) Influence of initial pH on the photolysis of TC (20 mg/L, irradiation time 60 min).

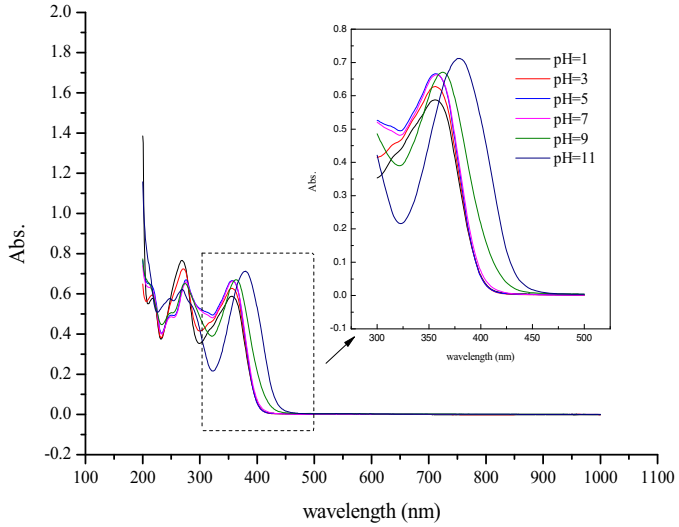

Fig. 10. The UV–vis spectra of TC at different pHs (20 mg/L).

absorption intensity were observed for TC. This was in concomitance with the transition of π–π^* state (HOMO-1 to LUMO) of chromophore [42,44], and the excited state was less stable and more prone to be photolyzed.

4. Conclusions

A novel three-dimensional (3D) mesoporous composite by hybridizing MWNTs with Bi_2WO_6 was successfully prepared using hydrothermal method. As the MWNTs could act as the trap of electrons from the conduction band of the Bi_2WO_6, it could improve the separation of the generated hole–electrons pairs and facilitate the photodegradation. The composite with 3% MWNTs exhibited the highest photoactivity under simulated sunlight irradiation, the degradation efficiency of which increased about 35% compared with bare Bi_2WO_6. In addition, the as-synthesized MWNTs–Bi_2WO_6 composite exhibited great adsorption to TC, promoting the contact of TC with and Bi_2WO_6. Although the TC (20 mg/L) in solution was completely degraded in one hour under simulated sunlight irradiation, the FT-IR and DTG analytical results indicated that the adsorbed TC was degraded after 3 h.

Acknowledgements

The authors gratefully acknowledge the financial support of Ministry of Science and Technology (2014CB932001, 2012ZX07529-003), Tianjin Municipal Science and Technology Commission (13JCZDJC35900), and the Ministry of Education Innovation Team (IRT 13024).

Appendix A. Supplementary data

Supplementary data associated with this article can be found, in the online version, at http://dx.doi.org/10.1016/j.apcatb.2015.03.043.

References

[1] E.E. Ghadim, F. Manouchehri, G. Soleimani, H. Hosseini, S. Kimiagar, S. Nafisi, PLoS One 8 (2013).
[2] A.L. Ling, N.R. Pace, M.T. Hernandez, T.M. LaPara, Environ. Sci. Technol. 47 (2013) 4046–4052.
[3] X.D. Zhu, Y.J. Wang, R.J. Sun, D.M. Zhou, Chemosphere 92 (2013) 925–932.
[4] L.L. Ji, W. Chen, L. Duan, D.Q. Zhu, Environ. Sci. Technol. 43 (2009) 2322–2327.
[5] Y. Chen, X. Cao, J. Kuang, Z. Chen, J. Chen, B. Lin, Catal. Commun. 12 (2010) 247–250.
[6] Y. Wang, X. Bai, C. Pan, J. He, Y. Zhu, J. Mater. Chem. 22 (2012) 11568.
[7] Y. Zuo, C. Wang, Y. Sun, J.S. Cheng, Mater. Lett. 139 (2015) 149–152.
[8] S.B. Zhu, T.G. Xu, H.B. Fu, J.C. Zhao, Y.F. Zhu, Environ. Sci. Technol. 41 (2007) 6234–6239.
[9] R. Hao, X. Xiao, X. Zuo, J. Nan, W. Zhang, J. Hazard. Mater. 209–210 (2012) 137–145.
[10] X. Yan, X. Wang, W. Gu, M. Wu, Y. Yan, B. Hu, G. Che, D. Han, J. Yang, W. Fan, W. Shi, Appl. Catal. B: Environ. 164 (2015) 297–304.
[11] C. Song, P. Chen, C. Wang, L. Zhu, Chemosphere 86 (2012) 853–859.
[12] Y. Hong, A. Ren, Y. Jiang, J. He, L. Xiao, W. Shi, Ceram. Int. 41 (2015) 1477–1486.
[13] C.Y. Wang, H. Zhang, F. Li, L.Y. Zhu, Environ. Sci. Technol. 44 (2010) 6843–6848.
[14] C. Chang, L. Zhu, Y. Fu, X. Chu, Chem. Eng. J. 233 (2013) 305–314.
[15] P. Ju, P. Wang, B. Li, H. Fan, S. Ai, D. Zhang, Y. Wang, Chem. Eng. J. 236 (2014) 430–437.
[16] J. Low, J. Yu, Q. Li, B. Cheng, Phys. Chem. Chem. Phys. 16 (2014) 1111–1120.
[17] C. Chang, Y. Fu, M. Hu, C. Wang, G. Shan, L. Zhu, Appl. Catal. B: Environ. 142–143 (2013) 553–560.
[18] C. Chang, L. Zhu, S. Wang, X. Chu, L. Yue, ACS Appl. Mater. Interfaces 6 (2014) 5083–5093.
[19] Z. Sun, J. Guo, S. Zhu, L. Mao, J. Ma, D. Zhang, Nanoscale 6 (2014) 2186–2193.
[20] H. Huang, H. Chen, Y. Xia, X. Tao, Y. Gan, X. Weng, W. Zhang, J. Colloid Interface Sci. 370 (2012) 132–138.
[21] D. Wang, Y. Zhen, G. Xue, F. Fu, X. Liu, D. Li, J. Mater. Chem. C 1 (2013) 4153.
[22] X. Li, R. Huang, Y. Hu, Y. Chen, W. Liu, R. Yuan, Z. Li, Inorg. Chem. 51 (2012) 6245–6250.
[23] S. Guo, X. Li, H. Wang, F. Dong, Z. Wu, J. Colloid Interface Sci. 369 (2012) 373–380.
[24] Y. Cui, H. Li, W. Hong, S. Fan, L. Zhu, Powder Technol. 247 (2013) 151–160.
[25] W. Sun, Z. Liu, C. Jiang, Y. Xue, W. Chu, X. Zhao, Catal. Today 212 (2013) 206–214.
[26] G. An, W. Ma, Z. Sun, Z. Liu, B. Han, S. Miao, Z. Miao, K. Ding, Carbon 45 (2007) 1795–1801.
[27] V. Datsyuk, M. Kalyva, K. Papagelis, J. Parthenios, D. Tasis, A. Siokou, I. Kallitsis, C. Galiotis, Carbon 46 (2008) 833–840.
[28] S.-W. Cao, X.-F. Liu, Y.-P. Yuan, Z.-Y. Zhang, Y.-S. Liao, J. Fang, S.C.J. Loo, T.C. Sum, C. Xue, Appl. Catal. B: Environ. 147 (2014) 940–946.
[29] J.G. Yu, G.P. Dai, B.B. Huang, J. Phys. Chem. C 113 (2009) 16394–16401.
[30] J. Zhang, J. Yu, M. Jaroniec, J.R. Gong, Nano Lett. 12 (2012) 4584–4589.
[31] G. Zhao, S. Liu, Q. Lu, F. Xu, H. Sun, J. Alloys Compd. 578 (2013) 12–16.
[32] H. Huang, H. Chen, Y. Xia, X. Tao, Y. Gan, X. Weng, W. Zhang, J. Colloid Interface Sci. 370 (2012) 132–138.
[33] B. Chai, T. Peng, P. Zeng, X. Zhang, Dalton Trans. 41 (2012) 1179–1186.
[34] K. Dai, T. Peng, D. Ke, B. Wei, Nanotechnology 20 (2009) 125603.
[35] Y. Ou, J. Lin, S. Fang, D. Liao, Chem. Phys. Lett. 429 (2006) 199–203.
[36] M.E. Parolo, M.J. Avena, G. Pettinari, I. Zajonkovsky, J.M. Valles, M.T. Baschini, Appl. Clay Sci. 49 (2010) 194–199.
[37] J. Yang, R. Miranda, C. Roy, Polym. Degrad. Stab. 73 (2001) 455–461.
[38] S. Dong, J. Feng, Y. Li, L. Hu, M. Liu, Y. Wang, Y. Pi, J. Sun, J. Sun, Appl. Catal B: Environ. 152–153 (2014) 413–424.
[39] P. Liu, Y. Guo, Q. Xu, F. Wang, Y. Li, K. Shao, Ceram. Int. 40 (2014) 5629–5633.
[40] Z. Li, L. Schulz, C. Ackley, N. Fenske, J. Colloid Interface Sci. 351 (2010) 254–260.
[41] M.E. Parolo, M.C. Savini, J.M. Vallés, M.T. Baschini, M.J. Avena, Appl. Clay Sci. 40 (2008) 179–186.
[42] S. Jiao, S. Zheng, D. Yin, L. Wang, L. Chen, Chemosphere 73 (2008) 377–382.
[43] J.J. López-Peñalver, M. Sánchez-Polo, C.V. Gómez-Pacheco, J. Rivera-Utrilla, J. Chem. Technol. Biotechnol. 85 (2010) 1325–1333.
[44] H.F. Dos Santos, E.S. Xavier, M.C. Zerner, W.B. De Almeida, J. Mol. Struct. Theochem 527 (2000) 193–202.